10.2 SIMULATION OF STRATOCUMULUS AND DEEP CONVECTIVE CLOUDS WITH THE DYNAMIC RECONSTRUCTION TURBULENCE CLOSURE

Xiaoming Shi[1]* Fotini Katopodes Chow[1], Robert L. Street[2] and George H. Bryan[3]

[1]University of California, Berkeley, CA
[2]Stanford University, Stanford, CA
[3]National Center for Atmospheric Research, Boulder, CO

1. INTRODUCTION

In recent years, the increase in computing power has enabled researchers to use high-resolution simulations to study convection in the atmosphere. However, these simulations are often in the so-called “terra incognita” (TI), or gray zone, of numerical simulation, where the size of the grid mesh is of the order of the scale of energetic eddies in the flow (Wyngaard, 2004). Since substantial amounts of energy are represented by the sub-filter scale (SFS) turbulence in these simulations, the formulation of turbulence closure models has great impact on the character of the simulated convection. Previous studies have shown that three-dimensional turbulence schemes designed for large-eddy simulations (LES) usually perform better than one-dimensional turbulence schemes designed for mesoscale models in the simulations of atmospheric convection (Parodi & Tanelli, 2010; Fiori et al., 2010; Verrelle et al., 2015; Machado & Chaboureau, 2015). However, while much effort has been devoted to understanding and improving turbulence closure for the simulations of dry convective boundary layer in the TI (Efstathiou & Beare 2015, Ito et al. 2015, Kitamura 2016, Shin & Dudhia 2016, Zhou et al. 2017), relatively few studies have examined the validity of LES-type turbulence schemes for simulating clouds and deep convection at TI resolutions.

Here, we compare traditional turbulence models and more advanced models using explicit filtering and reconstruction for the simulation of clouds. Two distinct cloud regimes are considered: stratocumulus clouds and deep tropical convective clouds. In each cloud regime, we examine how the character of the clouds and the resolved flow are affected by the choice of turbulence closure. The influence of turbulence models on simulations in the TI zone is also addressed. The LES code used in this study is the NCAR Cloud Model 1 [CM1, http://www2.mmm.ucar.edu/people/bryan/cm1/]. WENO schemes are used for the advection of momentum and scalars in CM1 for all our simulations.

2. TURBULENCE MODELS

Traditional turbulence models are based on eddy viscosities and diffusivities. SFS stress takes the following form,

$$\tau_{ij} = -2K_m S_{ij}\,, \tag{1}$$

where K_m is the eddy viscosity and S_{ij} is the strain rate tensor. Both the Smagorinsky model (SM) and the Deardorff 1.5 order turbulent kinetic energy closure model (TKE-1.5) have SFS stresses in forms similar to the equation above. In case of SM, K_m depends on deformation and stability. In the TKE-1.5 model, K_m is a function of a prognostic SFS kinetic energy and a stability-dependent length scale. The SFS mixing of scalars is determined similarly with an eddy diffusivity K_h and scalar gradients. In SM and TKE-1.5, $K_h = K_m/\mathrm{Pr}$ in effect, where Pr is the Prandtl number.

Dynamic models also use eddy viscosity/diffusivity based formulations as do traditional models, but the eddy viscosity and diffusivity are determined through dynamic procedures, for which we use the dynamic methods developed by Wong and Lilly (1994; DWL).

When explicit filtering is employed, the SFS motions are divided into resolvable subfilter scales (RSFS) and unresolvable subgrid scales (SGS), so SFS stress correspondingly has two parts. In the dynamic reconstruction model (DRM; Chow et al. 2005), which is based on the explicit filtering framework,

$$\tau_{ij} = -2K_m\bar{S}_{ij} + \left(\overline{\tilde{u}_i^*\tilde{u}_j^*} - \overline{\tilde{u}_i^*}\,\overline{\tilde{u}_j^*}\right) \tag{2}$$

where, the first term on the right is the SGS stress, and the second term in brackets is the RSFS contribution. The overline denotes the explicit filter, the tilde denotes the effects of the grid and discretization (see Carati et al. 2001). Here $\tilde{u}_i^*$ is the reconstructed velocity, which at the lowest order is set to $\bar{\tilde{u}}_i$, which is the resolved variable of an LES. The eddy viscosity K_m is determined with the dynamic Wong-Lilly (DWL) method.

In this work, DRM has two different versions, DRM-D and DRM-Pr. In DRM-D, eddy diffusivities for scalars are determined by independent dynamic procedures, while in DRM-Pr, an empirical formulation of turbulent Prandtl number (Venayagamoorthy and Stretch, 2010) is used to obtain eddy diffusivities based on the dynamically determined eddy viscosities.

The description of turbulence models above is brief, and further details are provided by Shi et al. (2017).

*Corresponding author address: Xiaoming Shi, O’Brien 205, University of California, Berkeley, CA 94720. Email: shixm@berkeley.edu

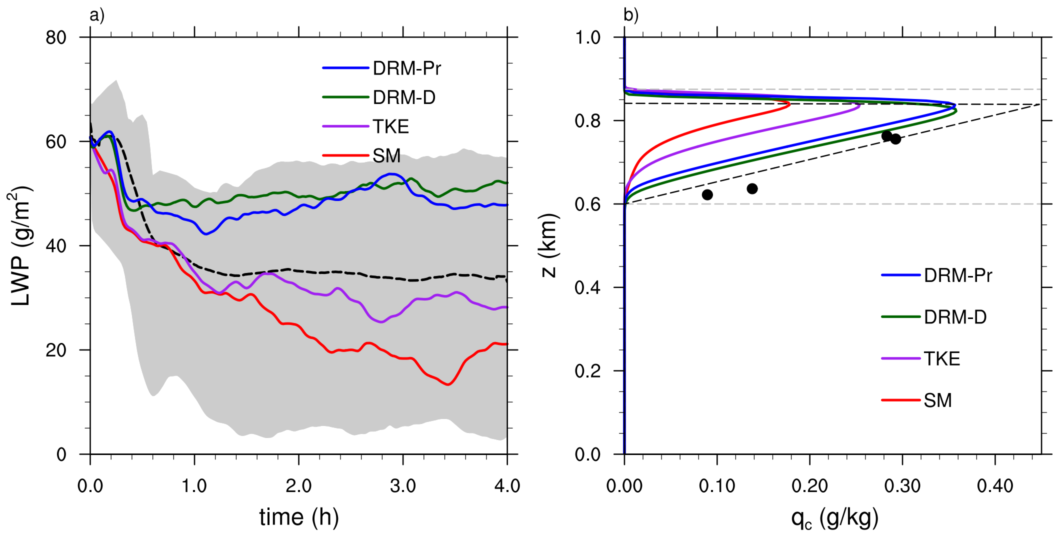

Figure 1: a) time series of liquid water path (LWP); b) the fourth hour mean profile of cloud water. Dashed black curve and gray shading in a) indicate the multi-model mean and spread of LWP in the intercomparison project of Stevens et al. (2005). Solid dots indicate *in-situ* observation from Stevens et al. (2005).

3 STRATOCUMULUS CLOUDS

For the stratocumulus cloud regime, we study the classic case of Stevens et al. (2005), which is based on the first research flight (RF01) of the second Dynamics and Chemistry of Marine Stratocumulus (DYCOMS-II) field study. The setup of our simulations follows the description in Stevens et al. (2005), including using the same idealized initial conditions and simplified radiative forcing. We first use their "standard" resolution, 5 m in the vertical and 35 m in the horizontal, to test the sensitivity of simulations to the turbulence closure model. Then we move onto TI resolutions to evaluate the performance of different turbulence schemes.

3.1 High-resolution simulations

Figure 1 compares the amount of cloud water in the simulations at the standard LES resolutions. Observation data suggest that liquid water path (LWP) in the simulations should maintain the value in the idealized initial condition, that is, about 60 g/m^2. However, as shown in Fig. 1a and b, using traditional models produces unrealistically thin cloud in the simulations. The Smagorinsky model exhibits the lowest value of LWP, and both the TKE-1.5 and Smagorinsky models exhibit less LWP than the multi-model mean of

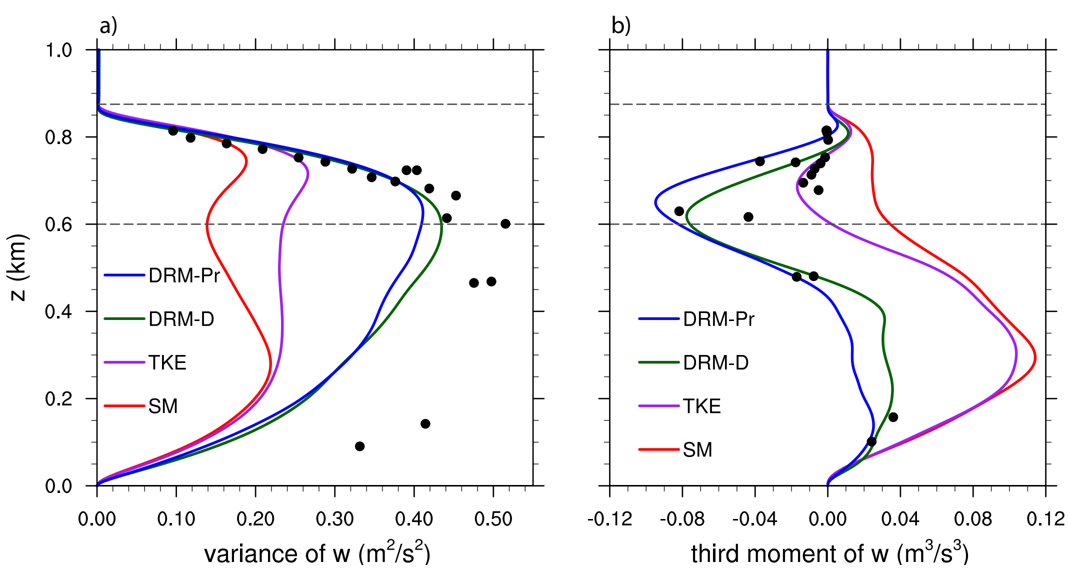

Figure 2： Fourth-hour mean of a) w variance and b) the third moment of w in the simulations. Dashed black lines indicate the height of cloud base and top. Solid dots indicate *in-situ* and radar observation from Stevens et al. (2005).

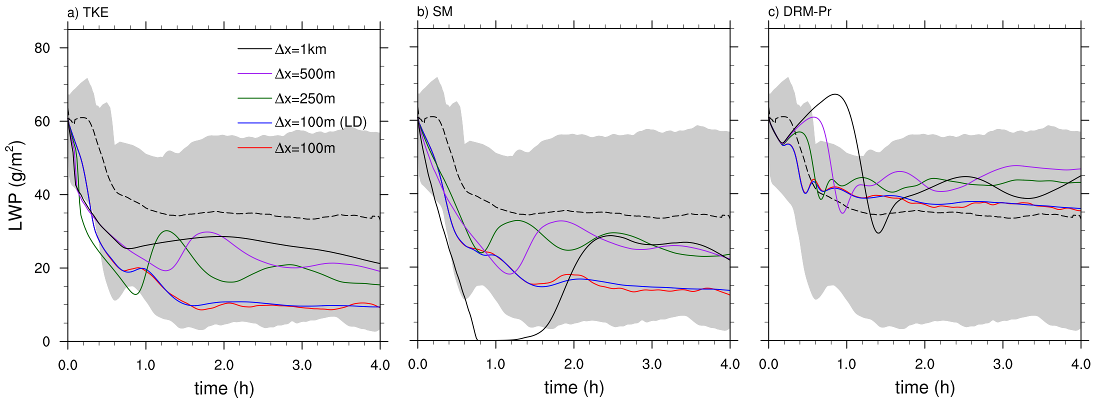

Figure 3: Liquid water path (LWP) of simulations using different turbulence closure schemes. Vertical spacing is 20m for all but different horizontal resolutions are used. LD denotes the large domain simulations with horizontal number of grid cells $n_x = n_y = 960$. All others have $n_x = n_y = 96$.

Stevens et al. (2015). In contrast, the two versions of DRM maintain significantly more cloud water. The fourth-hour mean LWP is roughly 50 g/m^2 in them. As shown in Fig. 1b, the amount of cloud water in DRM-D and DRM-Pr is much closer to the observed profiles of

cloud water than the TKE-1.5 and Smagorinsky models.

Figure 2 shows the variance and third moment of vertical velocity in the simulations. For variance, observation data indicate a single-peak profile with the maximum locating near cloud base. This profile suggests the boundary layer is vertically coupled and energetic eddies penetrate through the entire boundary layer. The simulations using DRM-Pr and DRM-D successfully capture the single-peak structure of w variance profile, though the variance near surface is not as strong as that in observation data. The TKE-1.5 and Smagorinsky models, on the other hand, exhibit much weaker variance and profiles having two local maxima. The double-peak structure is especially prominent in the simulation using the Smagorinsky model, and it indicates that the boundary layer is decoupled, with cloud-top cooling driven eddies and surface heating driven eddies coexisting in the boundary layer.

For the third moment of w, observation data indicate a profile with strong negative peak near the cloud base. The negative skewness indicates the presence of strong downdrafts, as expected in a flow predominantly driven by radiative cooling, whereas positive skewness indicates surface-heating driven turbulence and cumulus convection. The TKE-1.5 and Smagorinsky models exhibit profiles dominated by low-level positive skewness and missing the negative peak, suggesting clouds in these two cases are broken and do not provide sufficient radiative cooling. In contrast, DRM-D and DRM-Pr have profiles that match observation data very well. The profiles are dominated by negative peaks near the cloud base, suggesting turbulence in these cases is driven by strong cloud-top cooling.

Thus, at the fine resolution for this stratocumulus case, DRM-Pr and DRM-D produce much more realistic simulations for the stratocumulus-capped boundary layer, whereas traditional TKE-1.5 and Smagorinsky models fail to produce the correct structures by all the measures described above.

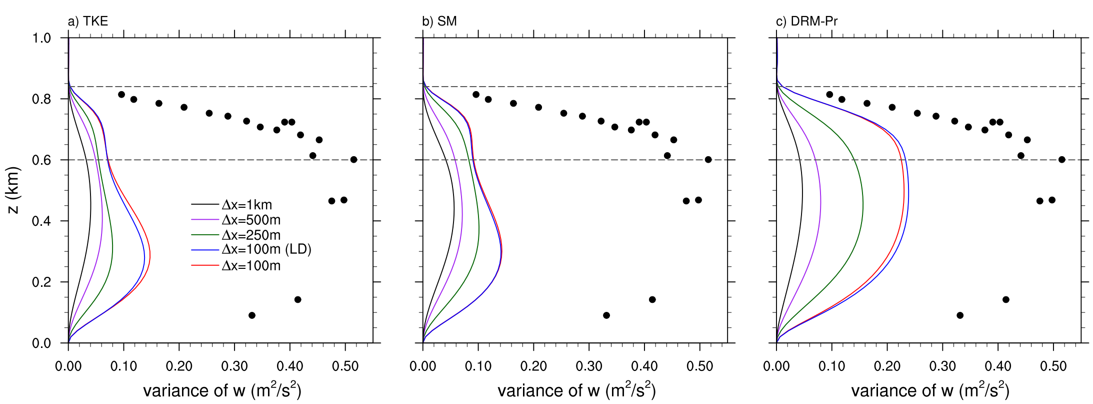

Figure 4: w variance in the simulations using different turbulence models and at varying horizontal resolutions.

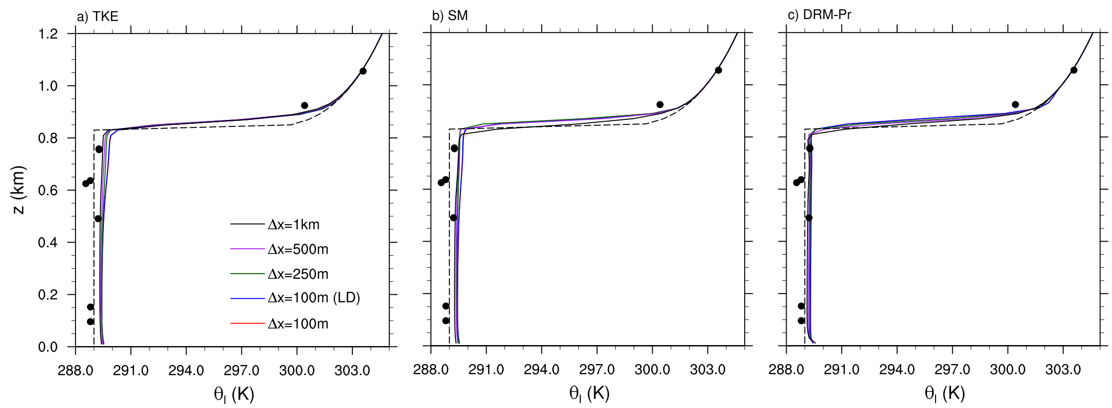

Figure 5: Liquid water potential temperature in the simulations using different resolutions and at varying horizontal resolutions.

3.2 Terra-incognita zone simulations

According to Pope (2000) and Matheou and Chung (2014), an LES should resolve 80 to 90% of the energy of the flow to obtain reliable statistics, which means the spacing of an LES grid mesh should be smaller than 1/12 or 1/32 times the integral scale of the flow (nominally the scale of the spectral peak). Since the vertical extent of the cloud is ~200 m, and the typical horizontal scale of stratocumulus cloud is ~10 km, we define the threshold resolution for the TI as 6.5–16.7m for the vertical and 312–833 m for the horizontal. A simulation with grid spacing equal to or larger than those thresholds is considered as a TI zone simulation.

First, we fix the horizontal grid spacing but vary the vertical grid spacing and compare the performance of the two versions of DRM. We find that DRM-Pr is significantly better than DRM-D in maintaining liquid water and boundary layer coupling at 20-m vertical resolution (not shown). Therefore, we choose DRM-Pr for further tests in which vertical resolution is fixed at 20m, and horizontal resolution is varied from 100m to 1km.

Figure 3 compares the simulations using TKE-1.5, Smagorinsky, and DRM-Pr turbulence models at varying horizontal resolutions. The TKE-1.5 and Smagorinsky models consistently produce less liquid water than the DRM-Pr scheme. The LWP in TKE-1.5 and Smagorinsky is always smaller than then multi-model mean (dashed curve in Fig. 3) of Stevens et al. (2005). The fourth-hour mean LWP of TKE-1.5 and Smagorinsky runs is only about 25 g/m^2 for the TI resolutions (500m and 1km). In contrast, DRM-Pr maintains LWP values greater than the mean of Stevens et al. and the fourth-hour mean is roughly 45 g/m^2.

Figure 4 shows w variance in the simulations using different turbulence closures at various resolutions. At 100 m and 250 m horizontal resolutions, DRM-Pr exhibit significantly more variance than the TKE-1.5 and Smagorinsky models, which exhibit double-peak structures and show stronger variance at lower levels while DRM-Pr exhibit single-peak profiles. At the TI resolutions, 500 m and 1 km, all turbulence models exhibit single-peak profiles, but the variance is very small compared with observations, suggesting that those resolutions are likely too coarse to resolve the details of boundary layer eddies.

Mean liquid water potential temperature profiles from different simulations are compared in Fig. 5. The DRM-Pr runs exhibit a well-mixed boundary layer for all the resolutions used, including the TI resolutions. In contrast, the TKE-1.5 and Smagorinsky runs exhibit a small amount of warm bias throughout the boundary layer, with slightly more warming in the cloud than below the cloud. The boundary layer is less well-mixed. Overall these mean profiles are relatively insensitive to resolution, but notably dependent on the subgrid turbulence model.

4 DEEP TROPICAL CONVECTION

For the deep convective cloud regime, we study the case originally used by Khairoutdinov et al. (2009). The initial conditions and the large-scale radiative and advection forcing for this case were derived from mean conditions during the GATE (Global Atmospheric Research Program (GARP) Atlantic Tropical Experiment) Phase III field experiment. Our simulation domain is 128 km in both horizontal directions and 25 km in the vertical direction. It is smaller than the original 200×200 km^2 domain used by Khairoutdinov et al. to save computational cost. For the control (high-resolution) runs, horizontal resolution is 100 m and the vertical resolution is variable, viz., 50 m below 1.25 km, stretched from 50 m to 100 m between 1.25 km to 5 km, and held constant at 100 m above 5 km. For coarse resolution simulations, the horizontal grid spacing is 500 m. In the vertical direction, the grid spacing is 100 m below 1 km, stretched from 100 m to 300 m between 1

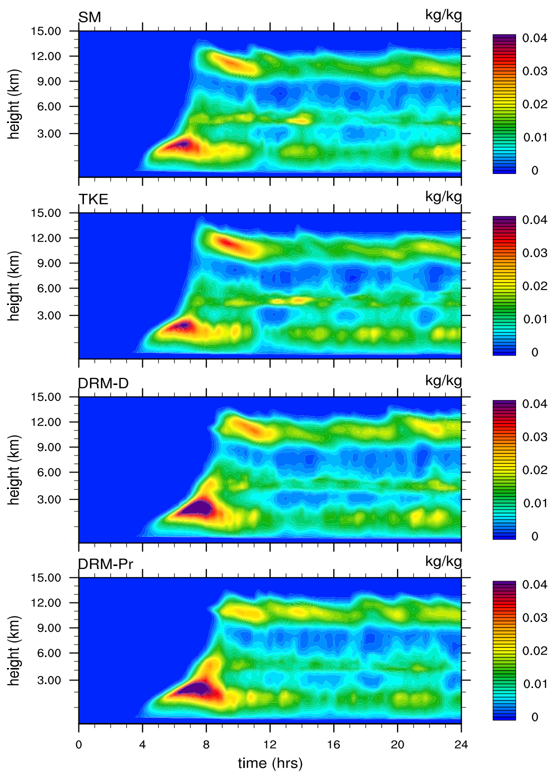

Figure 6: Horizontally averaged nonprecipitating cloud water and ice in the simulations of deep tropical convection with four different turbulence closure models.

km and 4 km, and 300 m above 4 km. Again, we compare four turbulence closure models in this cloud regime : Smagorinsky, TKE-1.5, DRM-D and DRM-Pr. For the Smagorinsky and TKE-1.5 models, additional versions using two different length scales for the vertical and horizontal directions are also tested at the coarse resolution. They are labeled SM2 and TKE2 in the analysis below.

4.1 High-resolution simulations

In this section, we examine the high-resolution simulations, which are the control runs. Figure 6 shows the nonprecipitating cloud water and ice in the simulations using different turbulence models. There is no cloud in the first four hours of the simulations, then shallow convection is triggered at about hour 4 and deep convection begins at about hour 8. The burst of convection in the simulations using DRM-D and DRM-Pr occurs about one hour later, compared the TKE-1.5 and Smagorinsky models. The initial convection between hour 4 and hour 8 in the DRM-D and DRM-Pr runs appears to be more intense than the initial convection in the TKE-1.5 and Smagorinsky runs. These differences result from the interaction between turbulence models and the random perturbations seeded in the initial conditions. However, once deep convection emerges, the distributions of cloud water and ice exhibit similar characters. Starting from hour 12, all the simulations

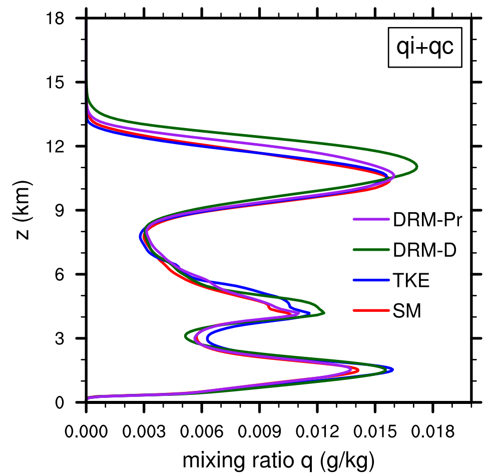

Figure 7: Last 8-hour mean profiles of nonprecipitating cloud water and ice.

enter quasi-equilibrium states, exhibiting tri-modal vertical distributions of cloud water/ice. This is consistent with the benchmark simulation of Khairoutdinov et al. (2009). Figure 7 compares the averaged profiles of nonprecipitating cloud water and ice in the last 8 hours of the simulations. Different turbulence closure models do not result in identical profiles, but the differences between them are relatively small. Thus, the resolution in the control simulations appears to be high enough to make the simulations insensitive to the choice of turbulence closure schemes.

Figure 8 shows characters of updraft and downdraft cores of convection and compares them with observation data. Here, following LeMone and Zipser (1980), a convective core is defined as a continuous region in the horizontal plane which has upward/downward velocities greater/smaller than +1/-1 m/s and has a minimum diameter of 500 m. The diameter of a core is defined as the minor axis length of the ellipse that encloses the updraft/downdraft region and has the same second moments as this region.

Figure 8a shows diameters of updraft/downdraft cores in the simulations. The median values of core diameters are only slightly larger than 500 m. The stronger, 90th percentile (i.e., the strongest 10%), cores have ~2 km diameters for updrafts and ~1 km diameters for downdrafts. For the strongest (99th percentile) convection, the updraft cores have diameters of about 4 to 6 km, and the downdraft cores have diameters of about 2 to 3 km. The distribution of core sizes matches observed diameters reasonably well. For the 50th and 90th percentiles, different turbulence models result in little spread in the diameter values. At the 99th percentile level, updraft core diameters exhibit small amount of differences between different turbulence models. The updraft core diameters in the simulation using DRM-D appear to be slightly larger than those in

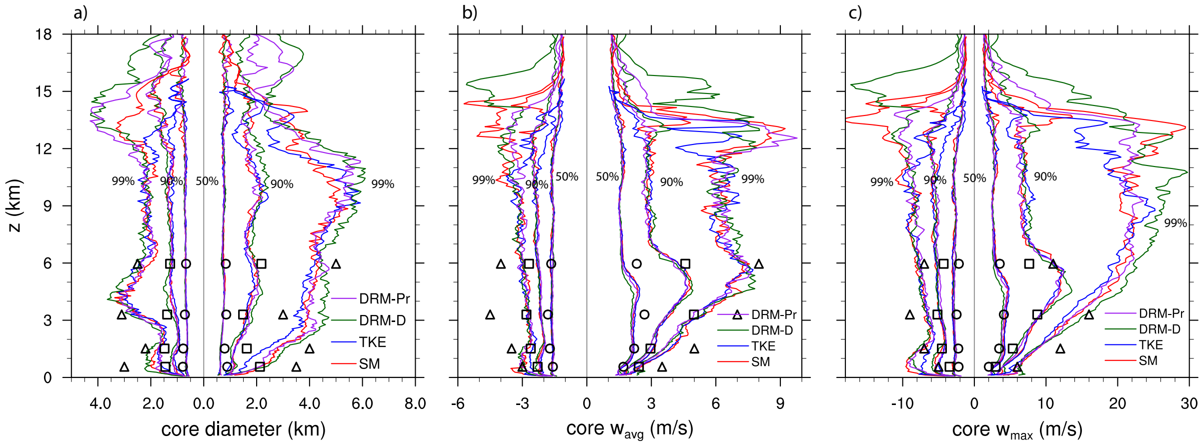

Figure 8: a) Diameter, b) mean speed, and c) maximum speed of updraft and downdraft cores of convection. In each panel, the left half is for downdraft and right half is for updraft. Values corresponding to different percentiles (50th, 90th, 99th) are shown in the figure. Markers indicate observed values (circles for 50th percentile, squares for 90th, and triangles for 99th) from LeMone and Zipser (1980).

other simulations. Above 12 km, the spread of core diameters among different simulations becomes large. However, overshooting convection reaching those altitudes is rather infrequent, so the spread at those altitudes may not be statistically significant.

Figure 8b shows mean velocities in updraft/downdraft cores. Different turbulence models show good agreement with each other below 12 km for all the percentiles. Updraft core strength is stronger than that of downdraft cores. The values of mean upward velocities match observations reasonably well, but downward velocities of cores are underestimated for the 90th and 99th percentile. Above 12 km, different turbulence models do not agree with each other, but again, results at those altitudes may not be statistically significant.

Maximum speeds of updraft and downdraft cores are shown in Fig. 8c. Data in the simulations and observation show good agreement. Upward motions are much stronger than downward motions, with strongest upward velocities reaching 20 m/s while downward velocities being smaller than 10 m/s. Updraft speeds for the 99th percentile show small spreads among different turbulence models in the middle and upper troposphere, while for others, the speed profiles resulting from different turbulence models overlay on each other. Disagreements on core velocities exist above 12km.

Overall, Figure 8 shows that convection core characteristics in the high-resolution control simulations agree well with the observed characteristics of convection during GATE III, and the simulations using different turbulence models also show good agreement with each other.

To measure the overall vertical transport caused by convection, we calculate some resolved fluxes from the simulations in Fig. 9. Figure 9a compares precipitation

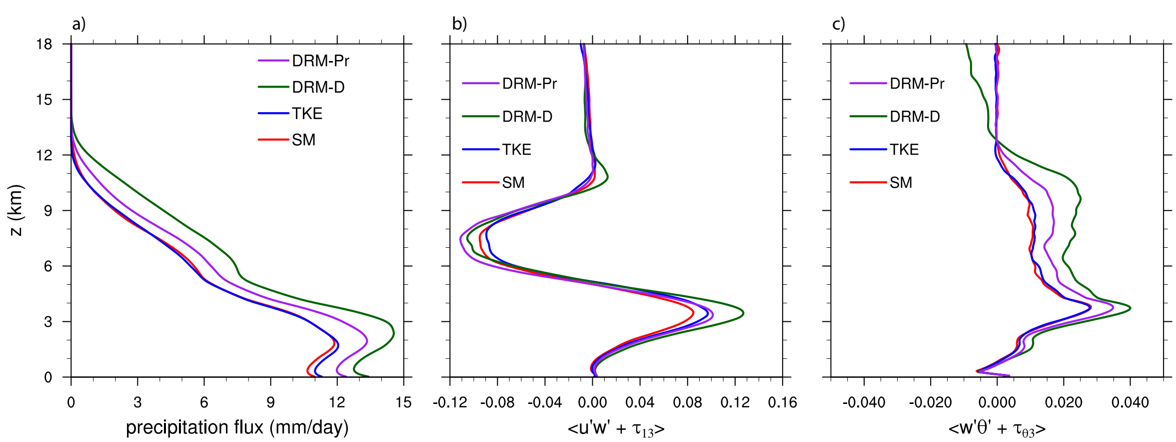

Figure 9: a) Precipitation flux, b) total (resolved+SFS) zonal momentum flux, and c) total (resolved+SFS) vertical heat flux in the simulations using different turbulence models.

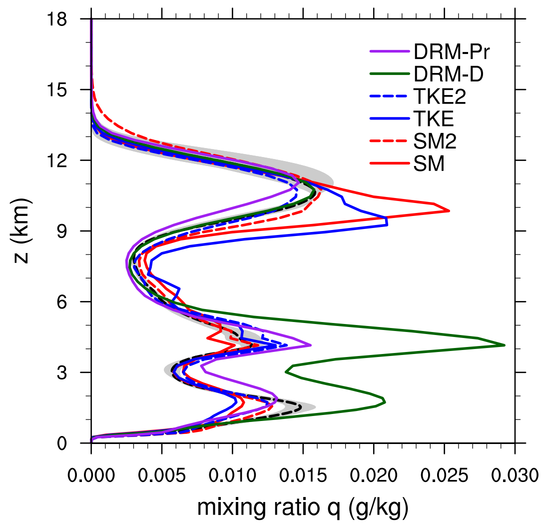

Figure 10: Mean profiles of nonprecipitating cloud water and ice in the coarse resolution simulations. TKE2 and SM2 indicate the TKE and Smagorinsky models in which two length scales are used for the horizontal and vertical directions separately. The black curve and gray shading indicate multi-model mean and spread from the high-resolution simulations.

fluxes in different runs. The simulation using DMR-Pr matches the previous simulation by Khairoutdinov et al. (2009; see their Fig. 11), while the simulations using the TKE-1.5 and Smagorinsky models produce slightly less precipitation flux, and the simulation using DRM-D yields slightly more precipitation. Figure 9b shows total (resolved and SFS) zonal momentum flux. Different simulations exhibit similar profiles, with small differences existing at 4 km and 7 km height for the positive and negative peaks of momentum flux. Lastly, total (resolved and SFS) vertical flux of heat is shown in Fig. 9c. The TKE-1.5 and Smagorinsky runs exhibit almost identical profiles of heat flux. The simulation using DRM-Pr produces slightly stronger heat flux than the TKE-1.5 and Smagorinsky runs, while the simulation using DRM-D exhibits significantly stronger heat transport, especially at the levels between 5 and 10 km.

Thus, overall, the inter-model spread for the simulations of deep tropical convection is modest at this resolution (100 m grid spacing). In the next section, we examine how coarsening model resolution may affect the properties of deep convection in the simulations.

4.2 Coarse resolution simulations

The coarse resolution runs examined here have 500 m grid spacing in the horizontal direction and variable vertical spacing as described above. For this case, we use the CM1 capability to use different length scales in the eddy viscosity computations, namely, the horizontal length scale is related to the horizontal grid resolution, while the vertical length scale is related to the vertical grid resolution. This practice is common in cloud-resolving models and accounts for both grid aspect ratio and physical eddy aspect ratio.

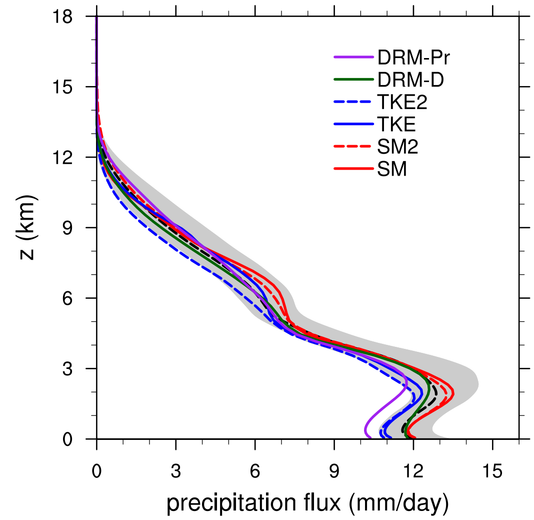

Figure 11: Same as Figure 10 but with mean profiles of precipitation flux.

In the previous section, we showed that the most intense (99th percentile) updraft cores have a diameter of ~6 km. Therefore, according to our standard of TI resolution (1/32 to 1/12 of the integral scale), the TI threshold for horizontal resolution is about 188 to 500m, and our simulations with 500 m are in the TI for deep convection.

Figure 10 compares the distribution of non-precipitating cloud water and ice in the coarse-resolution simulations. The Smagorinsky and TKE-1.5 models overestimate cloud ice at high levels compared to the multi-model mean of the high-resolution control simulations. DRM-D overestimates cloud water in the middle and lower troposphere. In contrast, the coarse resolution simulation using DRM-Pr stays close to the results of the high-resolution simulations. It is the best among all turbulence models using only a single length scale. When horizontal and vertical turbulence mixing are treated differently in SM2 and TKE2, the distribution of cloud water and ice is improved and also becomes similar to the high-resolution results.

Figure 11 shows precipitation flux profiles in the coarse-resolution simulations. None of the turbulence models departs substantially from the multi-model mean of high-resolution simulations. In the upper troposphere, TKE2, the TKE-1.5 model using two length scales, slightly underestimates precipitation flux. Near the surface, the precipitation rate in SM, SM2, and DRM-D matches the multi-model mean precipitation flux from high-resolution simulations, while the near-surface precipitation of TKE-1.5, TKE2 and DRM-Pr is smaller than the high-resolution simulation results.

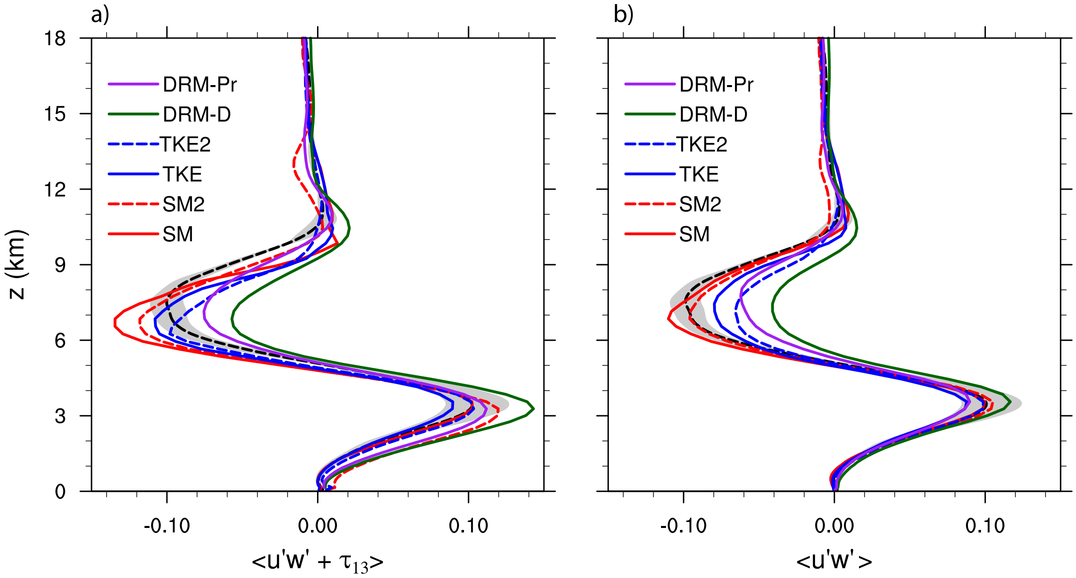

Figure 12: Mean profiles of a) total (resolved + SFS) and b) resolved zonal momentum flux in the coarse resolution simulations. TKE2 and SM2 indicate the TKE and Smagorinsky models in which two length scales are used for the horizontal and vertical directions separately. The black curve and gray shading indicate multi-model mean and spread from the high-resolution simulations.

Figure 12 shows mean total (resolved + SFS) zonal momentum flux in the coarse resolution simulations. Most turbulence models produce momentum flux profiles similar to the high-resolution results. DRM-D exhibits the largest underestimation compared to the multi-model mean at the level of ~7 km. SM and SM2 overestimate the negative flux peak at ~7 km, while DRM-Pr underestimates that negative flux peak. TKE and TKE2 exhibit the least errors at the level of ~7 km, but the height of the negative flux peak does not match the high-resolution results exactly. Figure 12b shows the resolved zonal momentum flux. Comparing Fig. 12a and 12b suggests that the total zonal momentum flux is dominated by the resolved flux. The effect of SFS momentum flux is noticeable but relatively small.

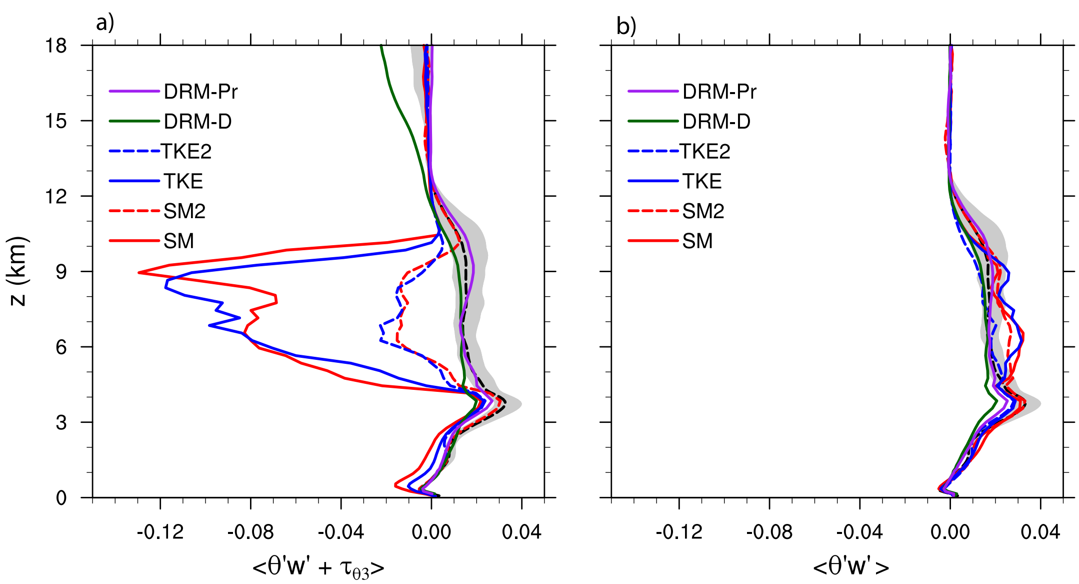

Figure 13: Mean profiles of a) total (resolved + SFS) and b) resolved vertical heat flux in the coarse resolution simulations. TKE2 and SM2 indicate the TKE and Smagorinsky models in which two length scales are used for the horizontal and vertical directions separately. The black curve and gray shading indicate multi-model mean and spread from the high-resolution simulations.

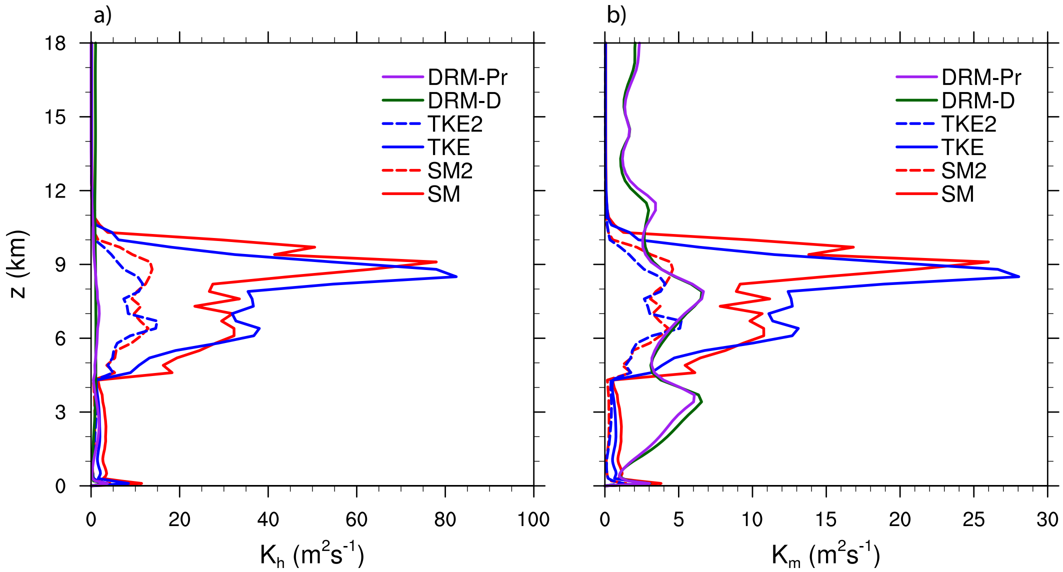

Figure 14: Mean profiles of a) eddy diffusivity for heat and b) eddy viscosity in coarse resolution simulations. TKE2 and SM2 indicate the TKE and Smagorinsky models in which two length scales are used for the horizontal and vertical directions separately.

Profiles of total (resolved + SFS) vertical heat flux are shown in Fig. 13a. Common practice is to use different horizontal and vertical length scales as noted above, but we show both cases here to highlight the impact of that choice and to contrast the SM and TKE-1.5 model behavior to that of the DRM models which use a single length scale, but dynamic coefficient determination. The most striking features appear in the coarse-resolution simulations using the TKE-1.5 and Smagorinsky models, which exhibit large amplitude excursions between 4 and 11 km. They show strong downward heat fluxes between 4 and 11 km in the coarse resolution simulations while the high-resolution simulations indicate total heat fluxes at those levels should be weakly positive. Treating vertical and horizontal turbulence mixing separately in SM2 and TKE2 reduces the amplitude of the excursions but does not remove them. In contrast, DRM-D and DRM-Pr do not have this behavior in the middle troposphere. Heat fluxes in coarse resolution simulations are still weakly positive. The DRM-D simulation exhibits weak negative heat flux above the tropopause, while other models indicate that at those upper levels total heat flux should be nearly zero.

Figure 13b shows mean profiles of resolved vertical heat fluxes in the coarse-resolution simulations. For all turbulence models, heat flux is positive at most levels and is between 0 and 0.04 K m s^{-1}. Therefore, the negative excursions of total heat flux in the coarse-resolution TKE-1.5 and Smagorinsky simulations are clearly produced by the contribution of the SFS turbulence models. The error above tropopause in the DRM-D simulation is also caused by the turbulence parameterization.

A further examination of eddy diffusivities and eddy viscosities in the simulations suggests that the TKE-1.5 and Smagorinsky models have unrealistically large eddy diffusivities and viscosities at the levels between 4 and 11 km in their coarse resolution simulations (Fig. 14). For example, the eddy diffusivities of the TKE-1.5 and Smagorinsky model have maxima of nearly 100 m^2s^{-1} in the middle troposphere of the coarse resolution simulations, while the eddy diffusivities of DRM-D and DRM-Pr in their coarse simulations are on the order of 1 m^2s^{-1} or smaller. When two length scales are used in SM2 and TKE2, eddy diffusivities become smaller but are still one order larger than the eddy diffusivities of DRM-D and DRM-Pr. DRM-D exhibits small but non-zero eddy diffusivity above the tropopause, while other models have zero diffusivities above the tropopause because of their built-in stability dependency. This nonzero value is responsible for DRM-D's heat flux errors above the tropopause, which can be avoided if a stability correction is applied to DRM-D (not shown).

Figure 14b suggests that the eddy viscosities in TKE and SM are also unrealistically large. The eddy viscosities do not produce large-amplitude effects in the SFS momentum flux because the mean wind shear is relatively small. For potential temperature, the mean vertical gradient is relatively large, so the SFS fluxes are large in most places when eddy diffusivity is large.

These results suggest that while the dynamic formulations can adapt to conditions in the TI, the traditional SM and TKE-1.5 have difficulty.

5. SUMMARY AND CONCLUSIONS

We compared the performance of four different turbulence models in two cloud regimes: the stratocumulus capped boundary layer and deep tropical convection. The Smagorinsky and TKE-1.5 models are two traditional models based on eddy viscosity/diffusivity, which are parameterized as a function of deformation rate and SFS TKE respectively. The two versions of DRM (DRM-D and DRM-Pr) contain two parts, one of which is the RSFS contribution based on reconstruction, the other of which is the SGS component based on dynamic eddy viscosity/diffusivity models.

For the stratocumulus capped boundary layer, the traditional turbulence models fail to maintain the proper amount of cloud water even at a fine LES resolution. In contrast, the distribution of cloud water in the simulations using DRM-D and DRM-Pr matches observations much better. Traditional models also fail in simulating a coupled boundary layer. Variance profiles of w exhibit double-peak structures in the simulations using the TKE-1.5 and Smagorinsky model, while profiles in the simulations using DRM-D and DRM-Pr have a well-defined single peak. In terms of w skewness, DRM-D and DRM-Pr successfully simulate the negative-peak dominating structure which exists in observation data, while the TKE-1.5 and Smagorinsky models produce profiles dominated by low-level positive skewness. When model resolution moves into the TI zone, DRM-Pr maintains significantly more cloud water than the TKE-1.5 and Smagorinsky models. The well-mixed boundary layer is maintained reasonably well in the simulations using DRM-Pr, while warm-biases develop in the simulations using traditional turbulence models.

For the simulations of deep tropical convection, the different turbulence models all produce consistent results at the 100-m resolution. All models produce a tri-modal distribution of nonprecipitating cloud water and ice. The characteristics of updraft and downdraft cores of convection match the observed characteristics of deep convection reasonably well. The vertical fluxes of precipitation, zonal momentum, and heat all are also consistent among the simulations using different turbulence models.

At coarser resolutions, the TKE-1.5 and Smagorinsky models exhibit large-amplitude excursions for vertical heat fluxes due to the SFS turbulence model component. It is found that the TKE-1.5 and Smagorinsky models have unrealistically large eddy viscosities and diffusivities in their coarse resolution simulations, and the large eddy diffusivities in particular lead to large-amplitude biases of downward heat flux. Splitting the calculation of horizontal and vertical eddy viscosity and diffusivity in the TKE-1.5 and Smagorinsky models reduce excursions in eddy diffusivities, but does not completely remove them. Though not shown here, large eddy diffusivities can likely also lead to errors in the transport of other scalars. In contrast, the two versions of DRM do not have large-amplitude biases for heat fluxes at 500 m resolution. DRM-D's performance is worse than DRM-Pr because DRM-D overestimates cloud water and produces false vertical heat fluxes above the tropopause. This deviation of DRM-D above the tropopause can be eliminated if a stability correction is applied, and we will implement such a correction in future versions of DRM. The overall performance of DRM-Pr is very satisfying in that its coarse-resolution simulations are more consistent with its high-resolution results.

The terra incognita of numerical simulations represents a challenging regime for the turbulence modeling. Energetic eddies are partially resolved, but substantial turbulent mixing is done by SFS processes. The results from both the stratocumulus and the deep convection cases demonstrate how traditional LES turbulence models have difficulty in the terra incognita for the simulations of clouds. The dynamic reconstruction model, which employs an explicit filtering and reconstruction framework, is a promising tool for modeling turbulence in the terra incognita.

Acknowledgments. This research was supported by National Science Foundation (NSF) Grants AGS 1503860 and AGS-1503885. We would like to acknowledge high-performance computing support from Yellowstone (ark:/85065/d7wd3xhc) provided by NCAR's Computational and Information Systems Laboratory, which is sponsored by NSF.

REFERENCES

Chow, F. K., R. L. Street, M. Xue, and J. H. Ferziger, 2005: Explicit filtering and reconstruction turbulence modeling for large-eddy simulation of neutral boundary layer flow. *J. Atmos. Sci.*, 62 (7), 2058–2077.

Efstathiou, G. A. and Beare, R. J., 2015: Quantifying and improving sub-grid diffusion in the boundary-layer grey zone. *Q.J.R. Meteorol. Soc.*, 141: 3006–3017. doi:10.1002/qj.2585

Fiori, E., A. Parodi, and F. Siccardi, 2010: Turbulence Closure Parameterization and Grid Spacing Effects in Simulated Supercell Storms. *J. Atmos. Sci.*, 67, 3870–3890.

Ito, J., Niino, H., Nakanishi, M. and Moeng, C.H., 2015. An extension of the Mellor–Yamada model to the terra incognita zone for dry convective mixed layers in the free convection regime. *Boundary-layer meteorology*, 157(1), pp.23-43.

Khairoutdinov, M. F., S. K. Krueger, C.-H. Moeng, P. A. Bogenschutz, and D. A. Randall, 2009: Large-Eddy Simulation of Maritime Deep Tropical Convection, *J. Adv. Model. Earth Syst.*, 1, 15.

Kitamura, Y., 2016. Improving a turbulence scheme for the terra incognita in a dry convective boundary layer. Journal of the Meteorological Society of Japan. Ser. II, 94(6), pp.491-506.
LeMone, M.A. and E.J. Zipser, 1980: Cumulonimbus Vertical Velocity Events in GATE. Part I: Diameter, Intensity and Mass Flux. J. Atmos. Sci., 37, 2444–2457.
Machado, L.A. and J. Chaboureau, 2015: Effect of Turbulence Parameterization on Assessment of Cloud Organization. Mon. Wea. Rev., 143, 3246–3262.
Matheou, G., and D. Chung, 2014: Large-eddy simulation of stratified turbulence. part ii: Application of the stretched-vortex model to the atmospheric boundary layer. J. Atmos. Sci., 71 (12), 4439–4460.
Parodi, A., and S. Tanelli, 2010: Influence of turbulence parameterizations on high-resolution numerical modeling of tropical convection observed during the TC4 field campaign, *J. Geophys. Res.*, 115, D00J14.
Pope, S. B., 2000: Turbulent flows. Cambridge University Press, 802 pp.
Shi, X., H. L. Hagen, Fotini K. Chow, George H. Bryan and Robert L. Street, 2017: Large-Eddy Simulation of the Stratocumulus-Capped Boundary Layer with Explicit Filtering and Reconstruction Turbulence Modeling, *J. Atmos. Sci.*, submitted.
Shin, H.H. and J. Dudhia, 2016: Evaluation of PBL Parameterizations in WRF at Subkilometer Grid Spacings: Turbulence Statistics in the Dry Convective Boundary Layer.*Mon. Wea. Rev.,* **144**, 1161–1177, https://doi.org/10.1175/MWR-D-15-0208.1
Stevens, B., and Coauthors, 2005: Evaluation of large-eddy simulations via observations of nocturnal marine stratocumulus. *Mon. Wea. Rev.*, 133 (6), 1443–1462,
Verrelle, A., Ricard, D. and Lac, C., 2015: Sensitivity of high-resolution idealized simulations of thunderstorms to horizontal resolution and turbulence parametrization. *Q.J.R. Meteorol. Soc.*, 141: 433–448.
Venayagamoorthy, S. K., and D. D. Stretch, 2010: On the turbulent Prandtl number in homogeneous stably stratified turbulence. *J. Fluid Mech.*, 644, 359–369.
Wong, V. C., and D. K. Lilly, 1994: A comparison of two dynamic subgrid closure methods for turbulent thermal convection. *Phys. Fluids*, 6 (2), 1016–1023.
Wyngaard, J. C., 2004: Toward numerical modeling in the “terra incognita”. *J. Atmos. Sci.*, 61, 1816–1826.
Zhou, B., K. Zhu, and M. Xue, 2017: A Physically Based Horizontal Subgrid-Scale Turbulent Mixing Parameterization for the Convective Boundary Layer. J. Atmos. Sci., 74, 2657–2674, https://doi.org/10.1175/JAS-D-16-0324.1